RESEARCH ARTICLE | AUGUST 30 2022

The influences of glass–glass interfaces and Ni additions on magnetic properties of transition-metal phosphide nano-glasses

Tian Li ; Guangping Zheng

AIP Advances 12, 085229 (2022)
https://doi.org/10.1063/5.0088043

The influences of glass–glass interfaces and Ni additions on magnetic properties of transition-metal phosphide nano-glasses

Cite as: AIP Advances 12, 085229 (2022); doi: 10.1063/5.0088043
Submitted: 16 February 2022 • Accepted: 5 August 2022 •
Published Online: 30 August 2022

Tian Li and Guangping Zheng[a)]

AFFILIATIONS

Department of Mechanical Engineering, The Hong Kong Polytechnic University, Hung Hom, Kowloon 10000, Hong Kong, China

[a)]Author to whom correspondence should be addressed: mmzheng@polyu.edu.hk

ABSTRACT

In this work, a novel kind of non-crystalline materials, the metallic nano-glasses (NGs), is synthesized, and the influences of glass–glass interfaces (GGIs) and Ni additions on the structural and thermodynamics properties, as well as the magnetism of (Co, Fe, Ni)–P NGs with various sizes of glassy grains (D_{avg}) are studied systematically. The addition of Ni and the reduction of D_{avg} are found to improve the glass forming abilities of NGs. The influences of volume fractions of GGIs on the magnetism of NGs are analyzed by Mössbauer spectroscopy and magnetization hysteresis measurements. It is found that the soft magnetic properties of (Co, Fe)–P NGs with reduced D_{avg} can be dramatically improved, as compared with micro-structured samples. Thus, this work has an in-depth understanding of the structural properties and magnetism of NGs as affected by the glass–glass interfaces in magnetic NGs.

I. INTRODUCTION

Due to their intrinsic structural characteristics, those metallic glasses (MGs), which are synthesized by rapid quenching, would normally possess outstanding soft magnetic properties[1] and have been studied extensively over the last several decades. However, the lack of microstructural defects (e.g., grain boundary and GB) has also greatly constrained the adjustment of magnetic behaviors of MGs since the microstructural refinement used today for polycrystalline materials can be no longer effective. As a result, current technological applications of MGs in electronic devices have still not reached a similar extent as those of crystalline alloys.[2]

Recently, a new type of non-crystalline materials, known as metallic nano-glasses (NGs), have been discovered, which consist of nano-sized amorphous grains surrounded by disordered glass–glass interfaces (GGIs).[3–7] Compared with melt-quenched MGs, GGIs possess unique atomic[8–10] and electronic[11] structures that could enable NGs with much different mechanical,[12–19] magnetic,[20–23] and thermodynamic[24–27] properties. For instance, Witte *et al.*[28] have discovered that heterogeneous Fe–Sc NGs exhibit to be ferromagnetic at room temperature while those homogeneous Fe–Sc MGs are found to be paramagnetic. It should be noted that elemental segregation at the interfacial regions cannot account for the ferromagnetism of GGIs since the Fe_xSc_{100-x} MGs have not been observed to be ferromagnetic at room temperature. In other words, a new glass phase, as two-dimensional defects, has formed in NGs. More importantly, in addition to manipulating their chemical compositions, the magnetic properties of NGs could be altered by adjusting the amount of GGIs as well. Therefore, size effects on the magnetic behaviors of NGs need to be well understood. Up until now, some studies[21,23,29,30] have investigated the magnetism of NGs, but a systematic understanding is still not available.

Similar to nanocrystalline (NCs) alloys, most NGs nowadays are manufactured through inert gas condensation,[31–33] magnetron sputtering,[34–36] and severe plastic deformation.[37–39] However, these techniques cannot be applied to prepare NGs with dimensions larger than centimeters economically. It is not until recently that pulse electrodeposition is utilized to fabricate NGs.[40] Compared with other methods, the cost of electrodeposition is low, and it can prepare NGs of various sizes and shapes for different purposes, especially for the application of magnetic NGs in power transformers with low

losses. So far, only a very few studies[41] have reported the preparation of NGs through electrodeposition. Moreover, it is known that soft magnetic properties of amorphous Co- and Fe-based alloys are superior,[42] and we have demonstrated, in our previous work,[41,43,44] that Co-based NGs containing other transition-metal elements can be fabricated using pulse electrodeposition, further improving their soft magnetic properties.

In the light of the aforementioned advantages of magnetic NGs containing transition-metal elements, in this work, Co–Fe–P and Co–Fe–Ni–P NGs are fabricated using the pulse electrodeposition method. The influences of GGIs and additions of alloying element Ni on the thermodynamic and magnetic properties of Co–Fe–P NGs are discussed. The NG samples with different GGI volume fractions are fabricated to investigate the effects of sizes of glassy grains on soft magnetic properties. The results clearly demonstrate that the soft magnetic properties of NGs can be dramatically altered by the GGIs as well as Ni additions.

II. EXPERIMENTAL METHODOLOGIES

The micro- and nano-structured samples with a thickness of up to 0.2 mm were prepared through electroplating in a conventional three-electrode electrochemical cell. Both Co–Fe–P and Co–Fe–Ni–P samples were deposited on a working electrode (WE), which was a titanium substrate polished to have a smooth surface. A graphite rod was used as a counter electrode (CE), and the working potential was controlled by a saturated calomel electrode (SCE). The composition of electrolytes was summarized as follows: $FeSO_4{\cdot}7H_2O$ with 0.03–0.06 mol/l, $CoSO_4{\cdot}7H_2O$ with 0.03–0.04 mol/l, $NiSO_4{\cdot}6H_2O$ with 0–0.03 mol/l, $C_6H_5Na_3O_7{\cdot}2H_2O$ with 0.2 mol/l, H_3BO_3 with 0.5 mol/l, and $NaH_2PO_2{\cdot}H_2O$ with 0.2 mol/l. The solution was maintained at 333 K throughout the deposition processes, and its pH was adjusted to be 3–4 by using concentrated sulfuric acid. Direct current electrodeposition with a working potential of 0.95 V was used to fabricate micro-structured samples. For the fabrication of nano-structured samples, pulse electrodeposition was adopted, and the working potential could be increased from 1.9 to 3.8 V, which reduced the sizes of glassy grains, thereby resulting in a higher amount of GGIs. A signal generator was used to output pulse signals with a fixed duty cycle of 15% at 100 kHz to the potentiostat. The duration of electroplating for micro- and nano-structured samples could be as long as 24 h. Self-designed Teflon molds were used to prepare 0.1 mm thick samples in a rectangular shape (30×3.5 mm^2) or in a ring shape (D_{outer} = 14 mm and D_{inner} = 10 mm). The as-prepared films were mechanically exfoliated from the substrate, and those free-standing specimens were heat-treated afterward in a tube furnace at 473 K in vacuum to release internal stresses.

The amorphous structures of Co–Fe–P and Co–Fe–Ni–P samples were characterized by x-ray diffraction (XRD, Rigaku Smartlab) operated at 45 kV and 250 mA with Cu K_α radiation (λ = 0.154 nm). Scanning electron microscopy (SEM, TESCAN VEGA3) equipped with energy dispersive spectroscopy (EDS) was utilized to observe the micro- or nano-structures in the cross sections of samples and determine the chemical compositions. High quality images of glassy grains with sizes less than 100 nm were taken by transmission electron microscopy (TEM, JOEL JEM-2011). Differential scanning calorimetry (DSC, TA Instruments Q200) was used to measure their thermodynamic properties at a heating rate of 10 K/min. The Mössbauer measurements were performed at 300 K using a conventional spectrometer (Germany, Wissel MS-500) in transmission geometry under constant acceleration mode. A ^{57}Co (Rh) source with an activity of 25 mCi was used. The velocity calibration was done with an α-Fe absorber at room-temperature. All spectra were fitted by the software Recoil using Lorentzian multiplet analysis. Physical properties measurement system (PPMS, Quantum Design) was used to measure the magnetic properties, and the isothermal magnetization curves were determined under applied magnetic fields of 0–10 kOe at room temperature. The complex permeability spectra of each specimen were measured by a radio frequency (RF) impedance analyzer (Agilent, 4294A) from 10^4 to 10^7 Hz.

III. RESULTS AND DISCUSSIONS

The SEM images of Co–Fe–P samples are shown in Figs. 1(a)–1(d). Based on the SEM images, the average sizes (D_{avg}) of glassy grains in Co–Fe–P samples are estimated to be 75 ± 9 nm, 125 ± 16 nm, 300 ± 29 nm, and 50 ± 7 μm by calculating the mean diameters of at least 20 grains, which are denoted as sample nos. 1–4, respectively. Similarly, as shown in Figs. 1(e)–1(h), D_{avg} = 80 ± 6 nm, 140 ± 13 nm, 280 ± 22 nm, and 40 ± 10 μm are determined for Co–Fe–Ni–P samples, which are denoted as sample nos. 1′–4′, respectively. It should be noted that sample nos. 4 and 4′ prepared through direction current (DC) electrodeposition processes are micro-structured glassy alloys since their glassy grains have sizes of 10–50 μm. Such a huge variation in D_{avg} of either Co–Fe–P or Co–Fe–Ni–P is attributed to different mechanisms in the formation of micro- and nano-structures. Compared with DC electrodeposition, cation sources for the growth of glassy grains are reduced in pulse electrodeposition by lowering the duty cycle. Meanwhile, the working potential in pulse electrodeposition is also much higher and can induce more nano-sized glassy clusters within a short period of time (~1 μs), which limits the space for the growth of glassy grains as well.

TEM images of NG sample nos. 1 and 1′ are illustrated in Figs. 2(a) and 2(b), respectively. It can be found that glassy grains with sizes less than 30 nm are formed in both samples. Moreover, their selected area diffraction (SAED) patterns with a halo ring indicate that the nanostructures synthesized by pulse electrodeposition are fully amorphous. The glassy grains in Co–Fe–Ni–P NGs seem to be more distinguishable as compared with those in Co–Fe–P NGs, suggesting that GGIs in the former may have atomic structures or chemical compositions much different from those in the interiors of glassy grains. It is thus speculated that the addition of Ni in Co–Fe–P NGs could be an effective approach in alternating the glass phase of GGIs in the NGs. Assuming that the thickness of GGIs is 1 nm and the glassy grains are spherical, the volume fractions of GGIs in Co–Fe–P sample nos. 1–4 are estimated to be 14.1%, 4.92%, 2.82%, and 0.01%, respectively, and those of GGIs in Co–Fe–Ni–P sample nos. 1′–4′ are 13.9%, 4.71%, 2.93% and 0.01%, respectively. The major difference between micro-structured glassy alloys and metallic glasses (MGs) is the structural heterogeneity in the former, which contains micro-size grained MGs as separated by the amorphous GGIs with a volume fraction of 0.01%. Table I summarizes the detailed information of Co–Fe–P and Co–Fe–Ni–P micro- and nano-structured samples prepared by electrodeposition.

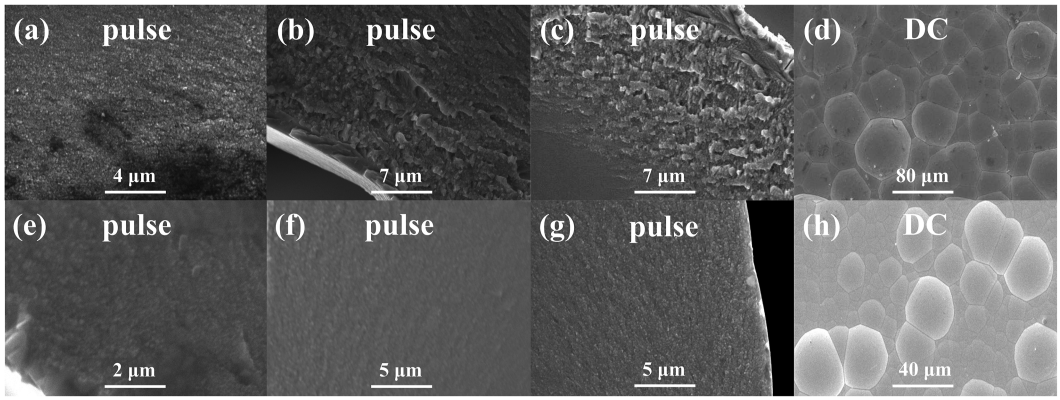

FIG. 1. (a)–(d) SEM images of Co–Fe–P sample nos. 1–4, respectively; (e)–(h) SEM images of Co–Fe–Ni–P sample nos. 1′–4′, respectively. The images are taken in the cross sections of samples, except that those in (d) and (h) are taken at the surfaces of micro-structured samples.

The room-temperature XRD patterns for Co–Fe–P and Co–Fe–Ni–P samples are shown in Figs. 3(a) and 3(b), respectively. A typical broad peak is found at $2\theta \sim 45^{\circ}$, and no sharp crystalline peak can be observed, suggesting both kinds of samples are fully amorphous, in consistent with the aforementioned TEM analyses. Meanwhile, compared with that of micro-structured samples (sample no. 4 with D_{avg} = 50 μm and sample no. 4′ with D_{avg} = 40 μm), an increase in the full width at half maximum diffraction peak is observed for nano-structured samples, suggesting that the glassy grains in the nano-structured samples could be several orders of magnitude smaller. In addition, the chemical compositions of Co–Fe–P and Co–Fe–Ni–P samples are found to be $Co_{65}Fe_{14}P_{21}$ and $Co_{58}Fe_5Ni_{14}P_{23}$ as determined by the EDS analyses, respectively, with all elements uniformly distributed in the micro- and nano-structured samples.

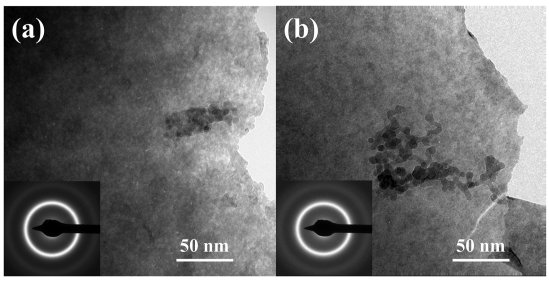

FIG. 2. TEM images and SAED patterns for (a) Co–Fe–P NG sample no. 1 and (b) Co–Fe–Ni–P NG sample no. 1′.

TABLE I. Chemical and physical properties of micro- and nano-structured samples prepared by electrodeposition.

Chemical compositions	Deposition conditions	D_{avg}	GGI volume fractions (%)	Labels
$Co_{65}Fe_{14}P_{21}$	Pulse	75 nm	14.1	Sample no. 1
	Pulse	125 nm	4.92	Sample no. 2
	Pulse	300 nm	2.82	Sample no. 3
	DC	50 μm	0.01	Sample no. 4
$Co_{58}Fe_5Ni_{14}P_{23}$	Pulse	80 nm	13.9	Sample no. 1′
	Pulse	140 nm	4.71	Sample no. 2′
	Pulse	280 nm	2.93	Sample no. 3′
	DC	40 μm	0.01	Sample no. 4′

Figures 4(a) and 4(b) show the heat-flow curves for Co–Fe–P and Co–Fe–Ni–P measured by DSC at a heating rate of 10 K/min, from which the crystallization temperatures (T_x) are determined at the sharp exothermic peaks in the curves, and the glass transition temperatures (T_g) are identified at the edges of endothermic shoulders of the heat flows. It can be found that at a fixed heating rate, T_x and T_g of Co–Fe–P and Co–Fe–Ni–P generally decrease with decreasing D_{avg}. In the previous studies on glassy polymer,[45–48] T_g is found to decrease as the sample sizes become smaller, resulting from the excess free volumes provided by the free surfaces. Similarly, in the Co–Fe–P and Co–Fe–Ni–P NGs, due to a higher content of free volumes at GGIs, a large volume fraction of GGI regions could be favorable for the glass transition, thereby lowering their T_g. In addition, GGIs could also facilitate crystallization transformation. At elevated temperatures, the decrease in T_x with increasing GGI volume fractions is consistent with the fact that crystalline clusters prefer to nucleate at GGIs where free volumes are enriched.

Figures 4(c) and 4(d) illustrate the dependence of T_g and T_x on D_{avg}, respectively. It is found that T_g of Co–Fe–P and Co–Fe–Ni–P samples with similar D_{avg} is nearly identical, which could be attributed to a similar level of free volumes at GGIs and interiors of glassy grains in the samples. In contrast, T_x is greatly influenced by the chemical compositions of samples. The decrease of T_x with the addition of alloying element Ni could be attributed to the formation of Ni–P nuclei with a lower energy barrier as compared with those for Co–P and Fe–P, thereby resulting in a supercooled liquid region ($T_x - T_g$) ~ 10 K narrower than those of Co–Fe–P samples with similar D_{avg}. Under a heating rate of 10 K/min, the enthalpy changes in glass transition (ΔH_g) are determined to be 34, 24.0, 22.5,

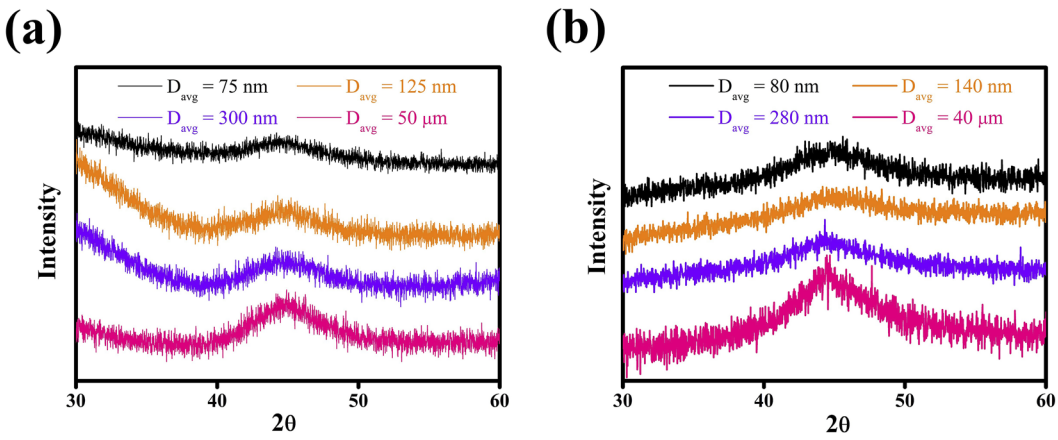

FIG. 3. XRD patterns for (a) Co–Fe–P sample nos. 1–4 and (b) Co–Fe–Ni–P sample nos. 1′–4′ with different D_{avg}.

and 20.4 J/g for Co–Fe–P sample nos. 1–4, respectively, while ΔH_g = 50.4, 48, 40, and 36 J/g for Co–Fe–Ni–P sample nos. 1′–4′, respectively. Therefore, the glass phase of GGIs in Co–Fe–Ni–P NGs could be more thermodynamically stable as compared with Co–Fe–P NGs because of the additions of Ni, and thus, Co–Fe–Ni–P NGs have higher glass forming abilities than Co–Fe–P NGs.

The room-temperature Mössbauer spectra for Co–Fe–P and Co–Fe–Ni–P samples with different D_{avg} are shown in Figs. 5(a)

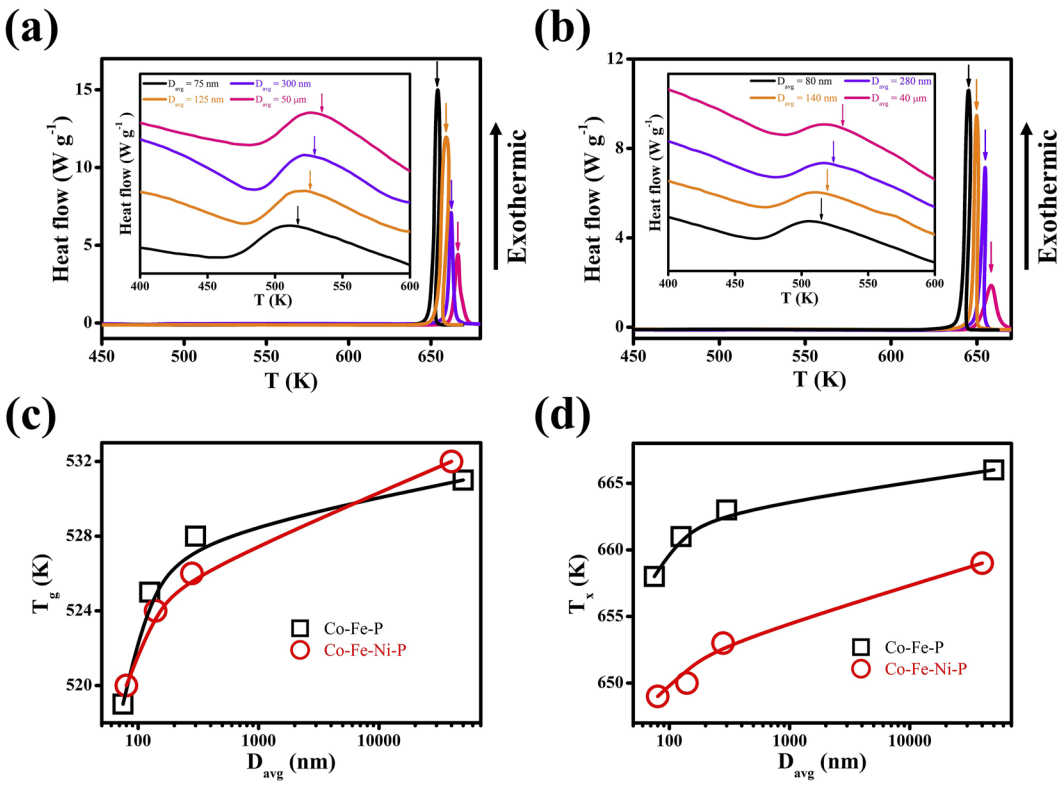

FIG. 4. DSC heat flows for (a) Co–Fe–P and (b) Co–Fe–Ni–P samples at a heating rate of 10 K/min. T_x and T_g are marked by arrows. The effects of Ni additions on (c) T_g and (d) T_x of the samples with different D_{avg} at a heating rate of 10 K/min.

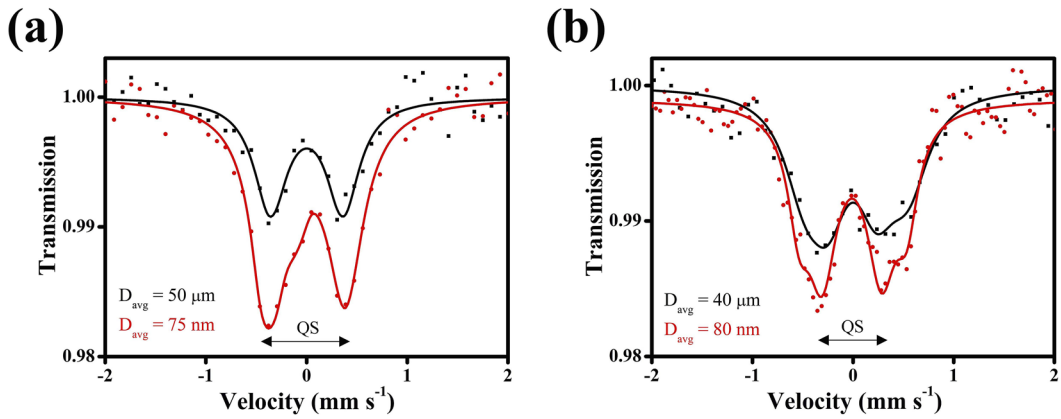

FIG. 5. Mössbauer spectra of micro- and nano-structured (a) Co–Fe–P sample no. 1 (D_{avg} = 75 nm) and sample no. 4 (D_{avg} = 50 μm), and (b) Co–Fe–Ni–P sample no. 1′ (D_{avg} = 80 nm) and no. 4′ (D_{avg} = 40 μm). The arrow indicates the quadruple splitting (QS) of a doublet.

and 5(b), respectively, manifesting a typical wide doublet for disordered structures in the samples. Compared with those for Co–Fe–P samples, the profile of doublet for Co–Fe–Ni–P samples exhibits an additional sub-peak located at ±0.5 mm/s, and it could be attributed to the Fe–Ni interaction in the samples. Furthermore, it can be found that the width of doublet for those nanostructured samples (sample nos. 1 and 1′) is broadened, which may be caused by the excess free volumes at GGI regions with large volume fractions in the samples. Since sample nos. 1 and 1′ have small D_{avg} and thus large volume fraction of GGIs, and the chemical environment of Fe atoms in these samples could be more heterogeneous than those of other samples, therefore, the width of doublet for sample nos. 1 and 1′ could be larger than those of other samples. Moreover, an increase in doublet intensity with reduced D_{avg} implies that the resonant atoms at GGI regions contribute to the signal significantly. Thus, the Mössbauer spectra suggest that the atomic and electronic structures of GGIs could be much different from those of glassy grains. In other words, the glass state and magnetism at GGIs could be different from those of glassy grains.

It should be noted that Mössbauer spectra could reveal the magnetism through quantitatively measuring the hyperfine interactions, which have three important types, including paired electron density at the nucleus, unpaired electron density at the nucleus, and electric field gradient (EFG) at the nucleus. Among them, EFG is often used to characterize the atomic and electronic structures around resonant atoms. Furthermore, the existence of EFG requires asymmetric structures around the nucleus, which can be reflected by the quadruple splitting (QS) of a doublet as indicated in Fig. 5. In general, a lower QS refers to less asymmetric structures, and the symmetric ones will induce only one resonance peak with QS = 0. For the micro-structured Co–Fe–P sample no. 4 and Co–Fe–Ni–P sample no. 4′, their QSs are measured to be 0.711 and 0.548 mm/s, respectively, whereas QSs are increased to 0.757 and 0.615 mm/s in nano-structured Co–Fe–P sample no. 1 and Co–Fe–Ni–P sample no. 1′, respectively. An increase in QS with increasing GGI volume fraction clearly illustrates the fact that GGIs are more disordered with distorted atomic and electronic symmetry as compared to glassy grains. In addition, previous studies[49] have proved that the glass forming abilities (GFAs) of MGs are enhanced with increasing QS values for (Fe, Co)-based MGs. The QS values for Co–Fe–P and Co–Fe–Ni–P samples with different D_{avg} thus suggest that the GGIs in NGs could become more thermodynamically stable with reduced D_{avg}.

Figures 6(a) and 6(b) show the isothermal magnetization curves for Co–Fe–P and Co–Fe–Ni–P samples with different D_{avg}, respectively. For Co–Fe–P sample nos. 1–4, their saturated magnetizations (M_s) are found to be 143, 129, 92, and 65 emu/g under an applied magnetic field of 10 kOe, respectively, whereas those of Co–Fe–Ni–P sample nos. 1′–4′ are reduced to 36, 35, 32, and 17 emu/g, respectively. Moreover, as measured from the magnetization hysteresis loops, the coercive field (H_c) of Co–Fe–P and Co–Fe–Ni–P samples with different D_{avg} are shown in Figs. 6(c) and 6(d), respectively. With increasing GGI volume fractions or decreasing D_{avg}, M_s and H_c of NGs would increase and decrease, respectively, which can be attributed to the distinct atomic and electronic structures of GGI regions as affected by their volume fractions, as analyzed by Mössbauer spectra. In other words, the magnetism of GGIs could much differ from those of glassy grains. Meanwhile, M_s and H_c of Co–Fe–Ni–P samples are found to be significantly decreased and increased as compared to those of Co–Fe–P samples with similar D_{avg}, also suggesting that the magnetism of GGIs in Co–Fe–Ni–P samples could be dramatically different from those in the corresponding Co–Fe–P samples after the addition of alloying element Ni. The results also demonstrate that the soft magnetic properties of Co–Fe–P NGs are superior and can be further improved by the reduction in D_{avg} without the addition of alloying element Ni.

To further investigate the size effects on the soft magnetic properties of NGs, complex permeability ($\mu = \mu' - j\mu''$) spectra as a function of frequency $f = 2\pi\omega$ of Co–Fe–P samples with different D_{avg} are measured as well, and the real permeability (μ') and imaginary permeability (μ'') can be calculated using the following equations:

$$\mu' = L_s/L_0 = L_s l_e/\mu_0 N^2 A_e, \quad (1)$$

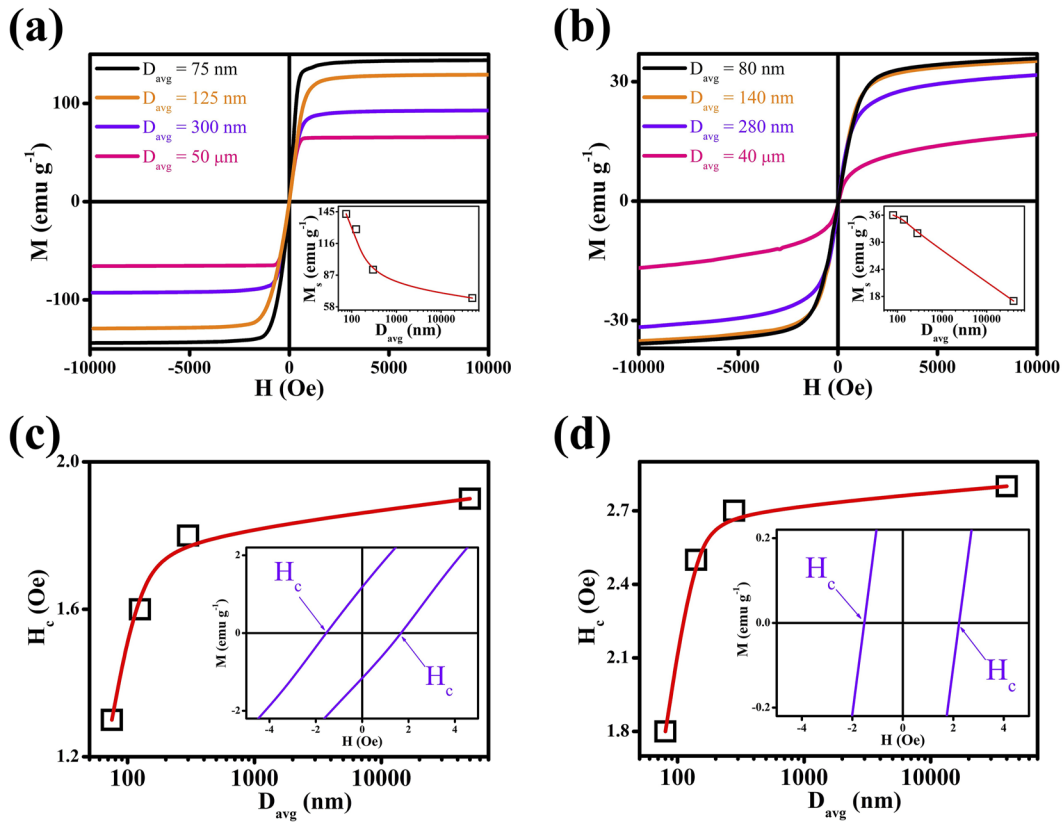

FIG. 6. Magnetization curves and coercive fields H_c at 300 K in (a) and (c), respectively, for Co–Fe–P, and in (b) and (d), respectively, for Co–Fe–Ni–P samples with different D_{avg}. The insets in (a) and (b) show M_s dependence on D_{avg}.

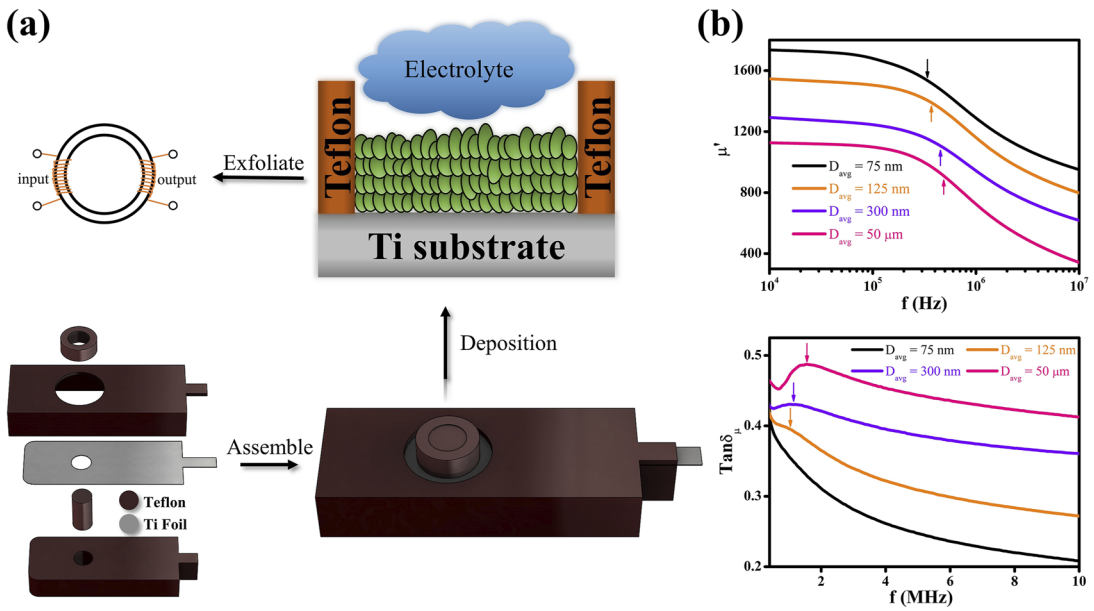

FIG. 7. (a) Schematics of preparation of ring-shaped Co–Fe–P samples for measuring complex permeability spectra. (b) Real permeability μ' and magnetic loss (tan δ_μ) for Co–Fe–P sample nos. 1–4 with different D_{avg}.

$$\mu'' = R_s/\omega L_0 = R_s l_e/\omega \mu_0 N^2 A_e, \quad (2)$$

where L_s is the self-inductance of sample core, R_s is the self-resistance of sample core, L_0 is the inductance of winding coils without sample core derived from geometry, N is the number of turns of the coils, A_e is the cross-sectional area, and l_e is the mean flux density path of a ring sample. Figure 7(a) illustrates the fabrication and the measurements of complex permeability spectra for the ring-shaped samples. As shown in Fig. 7(b), μ' of samples are found to increase with decreasing D_{avg}, suggesting that GGIs could much enhance the magnetism of NGs. Moreover, an apparent shift of resonance frequency (f_r) of μ', marked by arrows, toward lower frequencies with smaller D_{avg} or higher amounts of GGIs can be observed, which are attributed to Snoek's limit ($f_r \propto 1/\mu$).[50] Figure 7(b) also demonstrates the magnetic loss ($\tan\delta_\mu = \mu''/\mu'$) for sample nos. 1–4, which may be simply expressed as the sum of eddy current loss ($\tan\delta_e$), hysteresis loss ($\tan\delta_c$), and residual loss ($\tan\delta_r$) in the samples. However, $\tan\delta_e$ and $\tan\delta_r$, which are related to domain walls and spin rotational resonances, respectively, are typically small and are dependent on the electrical resistivity of the sample. Thus, the differences among $\tan\delta_e$ and $\tan\delta_r$ for sample nos. 1–4 could be negligible. Therefore, $\tan\delta_c$, which is related to H_c or the soft magnetic properties of Co–Fe–P samples, could dominate $\tan\delta_\mu$ of sample nos. 1–4. As can be seen in Fig. 7(b), $\tan\delta_\mu$ of nanostructured sample no. 1 is the lowest among all samples, which could be significantly reduced to ~0.2 at f = 10 MHz. With increasing D_{avg}, $\tan\delta_\mu$ at f = 10 MHz increases to ~0.27, ~0.36, and ~0.42 for sample nos. 2–4, respectively, resulting from the increase in their H_c as determined from the aforementioned magnetization hysteresis results. More importantly, for sample nos. 2–4, a prominent peak of $\tan\delta_\mu$, marked by arrows in Fig. 7(b), can be characterized at ~1.5 MHz. By subtracting the background of $\tan\delta_\mu$, the intensities of this peak for sample nos. 2–4 are estimated to be 0.006, 0.012, and 0.034, demonstrating that GGIs could have played an important role in the magnetic loss. The results further demonstrate that the soft magnetic properties could be much improved by forming NGs with D_{avg} < 100 nm where GGIs exist with a large volume fraction.

IV. CONCLUSION

In summary, micro- and nano-structured Co–Fe–P and Co–Fe–Ni–P samples with different D_{avg} are synthesized by DC and pulse electrodepositions. The effects of D_{avg} and the addition of alloying element Ni on the structural, thermodynamic, and magnetic properties of NGs are studied. The reduction in D_{avg} is found to improve the soft magnetic properties of NGs significantly. Mössbauer's analyses have demonstrated that the atomic and electronic structures of GGIs in the NGs are different from those of glassy grains, resulting in much lower magnetic losses in nano-structured Co–Fe–P samples.

ACKNOWLEDGMENTS

This work was supported by a grant from the Research Grants Council, University Grants Committee, Hong Kong (Grant No. PolyU152190/18E).

AUTHOR DECLARATIONS

Conflict of Interest

The authors have no conflicts to disclose.

DATA AVAILABILITY

The data that support the findings of this study are available from the corresponding author upon reasonable request.

REFERENCES

[1] L. Shi, X. Qin, and K. Yao, Prog. Nat. Sci.: Mater. Int. **30**, 208 (2020).
[2] A. Krings, A. Boglietti, A. Cavagnino, and S. Sprague, IEEE Trans. Ind. Electron. **64**, 2405 (2017).
[3] H. Gleiter, Beilstein J. Nanotechnol. **4**, 517 (2013).
[4] H. Gleiter, T. Schimmel, and H. Hahn, Nano Today **9**, 17 (2014).
[5] H. Gleiter, Small **12**, 2225 (2016).
[6] N. Chen, D. V. Louzguine-Luzgin, and K. Yao, J. Alloys Compd. **707**, 371 (2017).
[7] F. Tao, H. Hahn, and H. Gleiter, Acta Phys. Sin. **66**, 176110 (2017).
[8] J. X. Fang, U. Vainio, W. Puff, R. Würschum, X. L. Wang, D. Wang, M. Ghafari, F. Jiang, J. Sun, H. Hahn, and H. Gleiter, Nano Lett. **12**, 458 (2012).
[9] S. Lan, C. Guo, W. Zhou, Y. Ren, J. Almer, C. Pei, H. Hahn, C. T. Liu, T. Feng, X. L. Wang, and H. Gleiter, Commun. Phys. **2**(1), 117 (2019).
[10] X. Mu, L. Chen, R. Mikut, H. Hahn, and C. Kübel, Acta Mater. **212**, 116932 (2021).
[11] M. Ghafari, H. Hahn, H. Gleiter, Y. Sakurai, M. Itou, and S. Kamali, Appl. Phys. Lett. **101**, 243104 (2012).
[12] X. L. Wang, F. Jiang, H. Hahn, J. Li, H. Gleiter, J. Sun, and J. X. Fang, Scr. Mater. **98**, 40 (2015).
[13] X. Wang, F. Jiang, H. Hahn, J. Li, H. Gleiter, J. Sun, and J. Fang, Scr. Mater. **116**, 95 (2016).
[14] Q. Hu, J. Wu, and B. Zhang, Physica B **521**, 28 (2017).
[15] F. C. Li, T. Y. Wang, Q. F. He, B. A. Sun, C. Y. Guo, T. Feng, and Y. Yang, Scr. Mater. **154**, 186 (2018).
[16] C. Guo, Y. Fang, F. Chen, and T. Feng, Intermetallics **110**, 106480 (2019).
[17] C. Pei, R. Zhao, Y. Fang, S. Wu, Z. Cui, B. Sun, S. Lan, P. Luo, W. Wang, and T. Feng, J. Alloys Compd. **836**, 155506 (2020).
[18] A. Sharma, S. H. Nandam, H. Hahn, and K. E. Prasad, Scr. Mater. **191**, 17 (2021).
[19] T. Li and G. Zheng, Metall. Mater. Trans. A **52**, 1939 (2021).
[20] N. Chen, D. Wang, T. Feng, R. Kruk, K.-F. Yao, D. V. Louzguine-Luzgin, H. Hahn, and H. Gleiter, Nanoscale **7**, 6607 (2015).
[21] M. Ghafari, X. Mu, J. Bednarcik, W. D. Hutchison, H. Gleiter, and S. J. Campbell, J. Magn. Magn. Mater. **494**, 165819 (2020).
[22] A. Baksi, S. H. Nandam, D. Wang, R. Kruk, M. R. Chellali, J. Ivanisenko, I. Gallino, H. Hahn, and S. Bag, ACS Appl. Nano Mater. **3**, 7252 (2020).
[23] S. P. Singh, R. Witte, O. Clemens, A. Sarkar, L. Velasco, R. Kruk, and H. Hahn, ACS Appl. Nano Mater. **3**, 7281 (2020).
[24] O. Franke, D. Leisen, H. Gleiter, and H. Hahn, J. Mater. Res. **29**, 1210 (2014).
[25] J. Q. Wang, N. Chen, P. Liu, Z. Wang, D. V. Louzguine-Luzgin, M. W. Chen, and J. H. Perepezko, Acta Mater. **79**, 30 (2014).
[26] M. Mohri, D. Wang, J. Ivanisenko, H. Gleiter, and H. Hahn, J. Alloys Compd. **735**, 2197 (2018).
[27] S. H. Nandam, O. Adjaoud, R. Schwaiger, Y. Ivanisenko, M. R. Chellali, D. Wang, K. Albe, and H. Hahn, Acta Mater. **193**, 252 (2020).
[28] R. Witte, T. Feng, J. X. Fang, A. Fischer, M. Ghafari, R. Kruk, R. A. Brand, D. Wang, H. Hahn, and H. Gleiter, Appl. Phys. Lett. **103**, 073106 (2013).
[29] C. Wang, X. Mu, M. R. Chellali, A. Kilmametov, Y. Ivanisenko, H. Gleiter, and H. Hahn, Scr. Mater. **159**, 109 (2019).
[30] A. Stoesser, M. Ghafari, A. Kilmametov, H. Gleiter, Y. Sakurai, M. Itou, S. Kohara, H. Hahn, and S. Kamali, J. Appl. Phys. **116**, 134305 (2014).

[31]C. Wang, D. Wang, X. Mu, S. Goel, T. Feng, Y. Ivanisenko, H. Hahn, and H. Gleiter, Mater. Lett. **181**, 248 (2016).
[32]S. H. Nandam, Y. Ivanisenko, R. Schwaiger, Z. Śniadecki, X. Mu, D. Wang, R. Chellali, T. Boll, A. Kilmametov, T. Bergfeldt, H. Gleiter, and H. Hahn, Acta Mater. **136**, 181 (2017).
[33]S. P. Singh, M. R. Chellali, L. Velasco, Y. Ivanisenko, E. Boltynjuk, H. Gleiter, and H. Hahn, J. Alloys Compd. **821**, 153486 (2020).
[34]S. V. Ketov, X. Shi, G. Xie, R. Kumashiro, A. Y. Churyumov, A. I. Bazlov, N. Chen, Y. Ishikawa, N. Asao, H. Wu, and D. V. Louzguine-Luzgin, Sci. Rep. **5**, 7799 (2015).
[35]Z. Śniadecki, D. Wang, Y. Ivanisenko, V. S. K. Chakravadhanula, C. Kübel, H. Hahn, and H. Gleiter, Mater. Charact. **113**, 26 (2016).
[36]M. Mohri, D. Wang, J. Ivanisenko, H. Gleiter, and H. Hahn, Mater. Charact. **131**, 140 (2017).
[37]X. D. Wang, Q. P. Cao, J. Z. Jiang, H. Franz, J. Schroers, R. Z. Valiev, Y. Ivanisenko, H. Gleiter, and H.-J. Fecht, Scr. Mater. **64**, 81 (2011).
[38]H. Shao, Y. Xu, B. Shi, C. Yu, H. Hahn, H. Gleiter, and J. Li, J. Alloys Compd. **548**, 77 (2013).
[39]K. Wu, F. Chu, Y. Meng, K. Edalati, Q. Gao, W. Li, and H.-J. Lin, J. Mater. Chem. A **9**, 12152 (2021).
[40]C. Guo, Y. Fang, B. Wu, S. Lan, G. Peng, X.-l. Wang, H. Hahn, H. Gleiter, and T. Feng, Mater. Res. Lett. **5**, 293 (2017).
[41]T. Li, Y. Shen, and G. Zheng, Scr. Mater. **203**, 114109 (2021).
[42]D. Huang, Y. Li, Y. Yang, Z. Zhu, and W. Zhang, J. Alloys Compd. **843**, 154862 (2020).
[43]Y. Shen, X.-C. Zheng, and G.-P. Zheng, Metall. Mater. Trans. A **42**, 211 (2011).
[44]J. Cheng, T. Li, S. Ullah, F. Luo, H. Wang, M. Yan, and G. Zheng, Nanotechnology **31**, 385704 (2020).
[45]Q. Jiang and X. Y. Lang, Macromol. Rapid Commun. **25**, 825 (2004).
[46]J. L. Keddie, R. A. L. Jones, and R. A. Cory, Europhys. Lett. **27**, 59 (1994).
[47]D. Morineau, Y. Xia, and C. Alba-Simionesco, J. Chem. Phys. **117**, 8966 (2002).
[48]Q. Jiang, H. X. Shi, and J. C. Li, Thin Solid Films **354**, 283 (1999).
[49]Y. Lu, G. Huang, Z. Qin, X. Lu, and Y. Huang, Vacuum **141**, 173 (2017).
[50]Y. Bai, J. Zhou, Z. Gui, L. Li, and L. Qiao, J. Alloys Compd. **450**, 412 (2008).